Investigating Cavity Quantum Electrodynamics-Enabled Endo/Exo-Selectivities in a Diels-Alder Reaction

Jialong Wang,^{†,‡} Braden M. Weight,*,[¶] and Pengfei Huo*,^{†,§,}∥

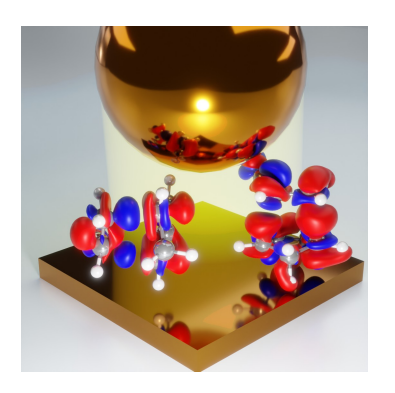
†Department of Chemistry, University of Rochester, Rochester, NY 14627, U.S.A. ‡Division of Arts and Sciences, NYU Shanghai, 567 West Yangsi Road, Shanghai 200124, China ¶Department of Physics and Astronomy, University of Rochester, Rochester, NY 14627, U.S.A. §The Institute of Optics, Hajim School of Engineering, University of Rochester, Rochester, NY 14627, U.S.A.

|| Center for Coherence and Quantum Science, University of Rochester, Rochester, New York 14627, U.S.A.

E-mail: bweight@ur.rochester.edu; pengfei.huo@rochester.edu

Abstract

Coupling molecules to a quantized radiation field inside an optical cavity has shown great promise in modifying chemical reactivity. Using the parameterized quantum electrodynamic (pQED) ab initio polariton chemistry approach, we theoretically demonstrate that the ground state selectivity of a Diels-Alder reaction can be fundamentally changed by strongly coupling this reaction to the cavity, generating preferential Endo or Exo isomers which are formed with equal probability for the same reaction outside the cavity. The numerical performance of pQED is in good agreement with the high-level self-consistent QED coupled cluster approach due to the exact light-matter interaction term used in pQED. By computing the ground state difference density, we show that the cavity induces a redistribution of electron density from intramolecular π -bonding orbitals to intermolecular bonding orbitals, thus providing chemical intuition of the cavity-induced changes to the ground state chemistry.



Introduction.

The Diels-Alder (DA) reaction, first elucidated in the previous century, stands as a cornerstone This cycloaddition reacof organic synthesis. tion involves the formation of a conjugated diene and a dienophile, typically an alkene, culminating in a substituted cyclohexene system. DA reactions are one of the most useful techniques for creating carbon-carbon bonds. 1,2 Furthermore, such reactions were fundamental in the Woodward-Hoffmann rules, ³ a set of principles governing the stereochemistry of organic reactions due to the symmetry of the molecular orbitals. A common feature of DA reactions is their capacity to result in either an "Endo" or "Exo" isomer during the formation of the transition state. This results in two distinct products. More specifically, if we consider the reaction between cyclopentadiene and acrylonitrile (see Fig. 1a), the resulting products under ambient conditions are known to provide Endo and Exo in equal proportion (i.e., no selectivity).

It was recently proposed that strong light-matter interactions between molecules and a quantized radiation field inside an optical cavity 4 are able to selectively produce one product over the other, due to the selective change of the transition state energy. While other techniques have been proposed to selectively form the Endo or Exo products, this novel pathway opens new directions for organic and inorganic synthesis which may pave the way for chemistry beyond what is currently accessible. However, in previous works, the molecules are placed in specific alignment with respect to the cavity polariza-

tion, and only a few calculations are performed due to the expensive QED coupled-cluster level of theoretical treatment.⁴

In this work, we use our efficient and accurate parametrized QED (pQED) approach^{5,6} to simulate how cavity QED can title the selectivities of a DA reaction. We demonstrate that the strong coupling between molecules and a cavity can fundamentally change a ground-state DA reaction. Our results suggest that one can fundamentally change the selectivity of this reaction from non-selective Endo/Exo products to highly selective Endo/Exo products by coupling this reaction inside an optical cavity. Our results obtained from pQED with linear response time-dependent density functional theory (TD-DFT) are comparable to highlevel results obtained from QED-coupled cluster. 4 Importantly, we further provide inuitive theoretical chemical insight into the cavity-induced changes to the ground state electron density ⁶⁻⁹ and relate the changes in density to the interplay between interand intra-molecular bonding orbitals, which are commonly used in the description of bond formation. ¹⁰ Furthermore, we compute all possible orientations of the molecule with respect to the cavity field polarization directions and identify the specific orientations of the molecule to the field polarization direction that maximize selectivity.

Our work demonstrates that strong coupling between molecules inside the cavity and the cavity photons offers a promising synthetic chemical tool. This coupling leads to cavity-induced changes to the ground state electron density and fundamentally modifies the outcome of known chemical reactions, making otherwise non-selective reactions selective. Our theoretical approach, pQED, offers an efficient and accurate way to simulate these reactions and provide direct chemical intuition via electron density modifications caused by coupling to the cavity.

Theoretical Methods.

We use the *ab initio* polariton approach, called parametrized-QED (pQED)⁵ to perform the calculations. The pQED approach uses the Pauli-Fierz (PF) Hamiltonian in the Born-Oppenheimer approximation (see Eq. 1) to describe light and matter interactions and use adiabatic electronic states as the basis for the electronic degrees of free-

dom and Fock states (*i.e.*, photon number states) as the basis for the photonic DOF. Specifically, we use the the Pauli-Fierz Hamiltonian in the dipole gauge $^{11-13}$ to investigate how cavity vacuum fluctuations induce modifications to the ground state. $^{4,5,5-11,13,13-21,21,22}$ The PF Hamiltonian is expressed as

$$\hat{H}_{\mathrm{PF}} = \hat{H}_{\mathrm{el}} + \hat{H}_{\mathrm{ph}} + \omega_{\mathrm{c}} A_0 \hat{\boldsymbol{\mu}} \cdot \hat{\mathbf{e}} (\hat{a}^{\dagger} + \hat{a}) + \omega_{\mathrm{c}} A_0^2 (\hat{\boldsymbol{\mu}} \cdot \hat{\mathbf{e}})^2,$$

$$\tag{1}$$

where $\hat{H}_{\rm el}$ is the electronic Hamiltonian under the Born-Oppenheimer approximation (without the nuclear kinetic energy operator), $\hat{H}_{\rm ph} = \omega_{\rm c} \hat{a}^{\dagger} \hat{a}$ is the Hamiltonian of the cavity field, \hat{a}^{\dagger} and \hat{a} are the raising and lowering operators of the cavity field, $\hat{\bf e}$ is a unit vector indicating the field polarization direction, and $\hat{\mu}$ is the dipole operator of the molecule. The last two terms in Eq. 1 are the light-matter coupling (electric dipole interaction) $\hat{H}_{\rm el-ph} = \omega_{\rm c} A_0 \hat{\mu} \cdot \hat{\bf e} (\hat{a}^{\dagger} + \hat{a})$ and the dipole-self energy (DSE) $\hat{H}_{\rm DSE} = \omega_{\rm c} A_0^2 (\hat{\mu} \cdot \hat{\bf e})^2$, respectively. Moreover, the light-matter coupling strength is expressed as

$$A_0 = \sqrt{\frac{1}{2\omega_c \epsilon \mathcal{V}}},\tag{2}$$

where ϵ is the permittivity inside the cavity, and \mathcal{V} is the effective mode volume. Alternatively, the electric field strength $\varepsilon = \omega_{\rm c} A_0$ can be used as a measure of coupling strength, which is common in experiments. In state-of-the-art cavity designs, such as those from gold or silver Nano-Particle-on-Metal (NPoM) cavities, the local electric field can vary from 1 to 10 V/nm, 23,24 which is well within the cavity parameters used in the present work. We chose $\omega_{\rm c}=1.5$ eV and the coupling strength $A_0=0.3$ a.u. that is equivalent to a mode volume $\mathcal{V}\sim0.19$ nm³ and field intensity of $\mathcal{E}\sim8.50$ V/nm, which the cavity frequency and field strength are experimentally achievable for plasmonic nano-cavity parameters. 23,24

As we discussed in our previous work, 5,6,13 the following two couplings in the Hamiltonian $^{11-13}$ shown in Eq. 1 cause the polariton ground states modifications. First, the off-resonance light-matter term $(\hat{H}_{\rm el-ph})$ couples through the ground state permanent dipole and transition dipoles between the ground and excited states. One simple example for the first case is the coupling between $|\psi_{\rm g},0\rangle$ and $|\psi_{\rm g},1\rangle$, which is proportional to $\langle\psi_{\rm g},0|\hat{\mu}(\hat{a}^{\dagger}+\hat{a})|\psi_{\rm g},1\rangle=\mu_{\rm gg}\langle 0|(\hat{a}^{\dagger}+\hat{a})|1\rangle=\mu_{\rm gg}$, and $|\psi_{\rm g},1\rangle$ will further couple to $|\psi_{\rm e},0\rangle$ through terms like $\langle\psi_{\rm e},0|\hat{\mu}(\hat{a}^{\dagger}+\hat{a})|\psi_{\rm g},1\rangle=\mu_{\rm ge}\langle 0|(\hat{a}^{\dagger}+\hat{a})|1\rangle$, where

 $\mu_{\rm gg}$ and $\mu_{\rm ge}$ are the permenant and transition dipoles among the ground and excited states, each projected along the cavity polarization direction $\hat{\bf e}$. The usual notion of hybrid light-matter states arise from this coupling term when the molecular ground state with one photon $|\psi_{\rm g},1\rangle$ and the excited molecular state with zero photons $|\psi_{\rm e},0\rangle$ become close in energy and hybridize into $|\Phi_{\rm e}\rangle \propto |\psi_{\rm g},1\rangle + |\psi_{\rm e},0\rangle$. 5,11

The second contribution is from dipole self-energy, which does not couple states of varying photon numbers but does provide non-trivial electronic couplings between ground and excited states. The DSE terms that couple to the ground state are proportional to $\langle \psi_{\rm g} | \hat{\mu}^2 | \psi_{\alpha} \rangle = \sum_{\gamma} \mu_{g\gamma} \mu_{\gamma\alpha}$, where α and γ include the ground and all excited electronic states. Overall, the direct coupling term $\hat{H}_{\rm el-ph}$ and $\hat{H}_{\rm DSE}$ both contribute to modifications to the ground state. 5,6,13,16,25–28 Through these non-resonant light-matter couplings, the cavity induces modifications to the reactions that are beyond the prediction of the simple Jaynes-Cummings model. ²⁹

The polariton eigenstates and eigenenergies are obtained by solving the following eigenvalue equation

$$\hat{H}_{PF}|\Phi_{i}(\mathbf{R})\rangle = E_{i}(\mathbf{R})|\Phi_{i}(\mathbf{R})\rangle,$$
 (3)

where \hat{H}_{PF} is given in Eq. 1, $E_j(\mathbf{R})$ is the Born-Oppenheimer polaritonic potential energy surfaces (PES) (which parametrically depend on the nuclear coordinates \mathbf{R}), and $|E_j(\mathbf{R})\rangle$ is the adiabatic polariton state. We directly diagonalize the polaritonic Hamiltonian \hat{H}_{PF} matrix and obtain the eigenvalues. The basis is constructed using the tensor product of electronic adiabatic states $|\psi_{\alpha}(\mathbf{R})\rangle$ (i.e., eigenstates of the electronic Hamiltonian $\hat{H}_{el}|\psi_{\alpha}(\mathbf{R})\rangle = \mathcal{E}_{\alpha}(\mathbf{R})|\psi_{\alpha}(\mathbf{R})\rangle$) and the Fock states $|n\rangle$ (i.e., eigenstates of the photonic Hamiltonian $\hat{H}_{ph}|n\rangle = n\omega_c|n\rangle$), expressed as $|\psi_{\alpha}(\mathbf{R})\rangle \otimes |n\rangle \equiv |\psi_{\alpha}(\mathbf{R}), n\rangle$. This basis is used to evaluate the matrix elements of \hat{H}_{PF} , and diagonalizing it provides $E_j(\mathbf{R})$ and the corresponding polariton states

$$|\Phi_j(\mathbf{R})\rangle = \sum_{\alpha}^{N_{\rm el}} \sum_{n}^{N_{\rm F}} C_{\alpha n}^j |\psi_{\alpha}(\mathbf{R}), n\rangle,$$
 (4)

where $C_{\alpha n}^{j} = \langle \psi_{\alpha}(\mathbf{R}), n | \Phi_{j}(\mathbf{R}) \rangle$. Here, the number of included electronic states, $\mathcal{N}_{\mathrm{el}}$, and photonic Fock/number states, \mathcal{N}_{F} , are treated as convergence parameters.

In the Diels-Alder reaction investigated in this

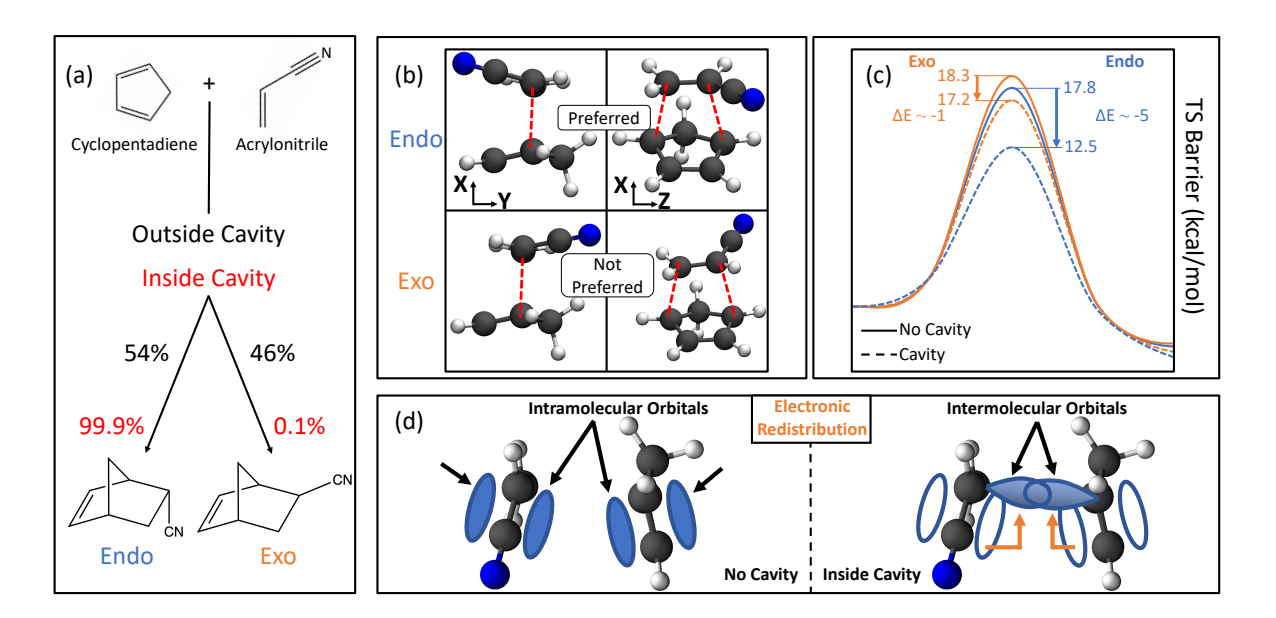
work, the numbers of states we used to solve the Eq. 3 are $\mathcal{N}_{\rm F}=10$ and $\mathcal{N}_{\rm el}=50$. We use the light-matter coupling strength $A_0=0.3$ a.u. and coupling frequency $\omega_{\rm c}=1.5$ eV to perform the reaction. We have carefully checked the convergence of the calcualiton following the procedure outlined in our previous works. ^{5,6} Further details regarding the pQED approach and higher coupling frequency results are provided in the **Supporting Information**.

All electronic structure computations were performed using the Q-CHEM software package.³⁰ We employed the parametrized quantum electrodynamics time-dependent density functional theory (pQED-TDDFT) approach with the ω B97XD hybrid exchange-correlation functional and the 6-311+G** basis set. When aligning the cavity polarization direction ê with a specific molecular axis, either $\hat{\mathbf{e}} = \mathbf{X}$ or $\hat{\mathbf{e}} = \mathbf{Y}$, or $\hat{\mathbf{e}} = \mathbf{Z}$, the matrix elements $\langle \psi_{\alpha} | \hat{\boldsymbol{\mu}} \cdot \mathbf{X} | \psi_{\gamma} \rangle$ and $\langle \psi_{\alpha} | \hat{\boldsymbol{\mu}} \cdot \mathbf{Y} | \psi_{\gamma} \rangle$ are input for the interaction term $\hat{\boldsymbol{\mu}} \cdot \hat{\mathbf{e}}$ and for the DSE term. For the cavity polarization direction in a general case (see Fig. 4), the interaction term follows the relationship $\hat{\mathbf{e}} \cdot \hat{\boldsymbol{\mu}} = \sin \theta \cos \phi \ \mathbf{X} \cdot \hat{\boldsymbol{\mu}} + \sin \theta \sin \phi \ \mathbf{Y} \cdot \hat{\boldsymbol{\mu}} +$ $\cos\theta \ \mathbf{Z} \cdot \hat{\boldsymbol{\mu}}$. Both ground state energies and electron density differences were determined using the Q-CHEM package. ³⁰

Results and Discussions.

We investigate the DA reaction between cyclopentadiene and acrylonitrile (Scheme 1a). This reaction produces two distinct Endo/Exo isomers as products. Outside the cavity and under standard reaction conditions, the DA reaction is kinetically controlled and shows a non-selective result with 54% Endo to 46% Exo products. It has been recently proposed 4 that this intrinsically non-selective reaction can be made selective by coupling the ground state of the reacting molecules to an optical cavity with frequency in the range of electronic excitations (i.e., $\omega_c \sim 1-3$ eV) in contrast to the recently explored vibrational strong coupling regime 31,32 (i.e., $\omega_c \sim 0.1$ eV).

Scheme 1 highlights the main results of this work, with the reaction depicted in panel (a). Panel (b) shows the transition states (TS) of this reaction that lead to the Endo (top) or the Exo (bottom) products. The red dashed lines between the molecules show the bonds that will form upon



Scheme 1: (a) Schematic representation of the Diels-Alder reaction between cyclopentadiene and acrylonitrile. The percent distribution of products is shown for the outside (black) and inside (red) of the cavity. ⁴ (b) Transition state (TS) geometries for both Endo (top) and Exo (bottom) pathways at two different orientations. (c) The TS barrier energy inside (dashed) and outside (solid) for the Endo (orange) and Exo (blue) reaction pathways. The cavity polarization is aligned with the Y-direction with light-matter coupling strength $A_0 = 0.3$ a.u. and $\omega_c = 1.5$ eV. (d) Schematic illustration showing the cavity-induced redistribution of electron density from intramolecular orbitals to intermolecular ones, thus facilitating an intermolecular bond and lowering the TS barrier energy.

the reaction. Furthermore, we emphasize that the Endo pathway becomes preferred inside the cavity under experimentally feasible cavity conditions, even in the presence of orientational disorder of the molecule with respect to the cavity field polarization direction. As suggested in Ref. 4 (and confirmed in the current work), the selectivity shifts to 99.9% for the Endo product and only 0.1%for the Exo. As an example of the modifications to the PES, we show the ground state PES in Scheme 1c, where the reactant (R) and TS geometries of the Endo (blue) and Exo (orange) isomers are placed inside the cavity with the cavity polarization along the Y-direction of the molecule. In this case, there is a significant change of the selectivity toward Endo species through a reduction of the TS barrier height by ~ 5 kcal/mol for the Endo and ~ 1 kcal/mol for the Exo compared to outside the cavity. This shifts the expected yields of the reaction to 99.9% and 0.1% for the Endo and Exo isomers, respectively, consistent with previous work in Ref. 4. In this case, our pQED-TDDFT calculations quantitatively reproduced the scQEDcoupled cluster with singles and doubles excitations (QED-CCSD) approach, 4 with more details

and comparisons to be discussed in Fig. 2. This shift in selectivity can be understood as cavity-induced electronic redistribution under the influence of the cavity (Scheme 1d). More specifically, coupling to the cavity induces electron density to be taken from occupied intramolecular π -bonding orbitals (*i.e.*, single-particle orbitals) to virtual intermolecular orbitals, thus facilitating a reduction in energy of the TS barrier height.

Fig. 1 presents the X-, Y-, and Z-directions of cavity field polarization using the TS geometries provided in Ref. 4. Fig. 1 shows the TS barrier height $E^{\ddagger} = E_0(\mathbf{R}_{TS}) - E_0(\mathbf{R}_{reac})$ in the ground polaritonic state $|\Phi_0(\mathbf{R})\rangle$ as a function of the lightmatter coupling strength A_0 for the three primary cavity field polarization directions, (blue) X, (orange) Y, and (green) Z, for the (a) Endo and (b) Exo isomers. In both the Endo and Exo pathways (Fig. 1), the TS barrier increases for the Xpolarized cavity (blue curve) by 7.2 kcal/mol and 6.7 kcal/mol at $A_0 = 0.3$ a.u., respectively, compared to outside the cavity ($A_0 = 0.0$ a.u.). The X-polarized cavity is not expected to offer selectivity for this reaction due to the simultaneous and unfavorable increase in TS barrier energy for the

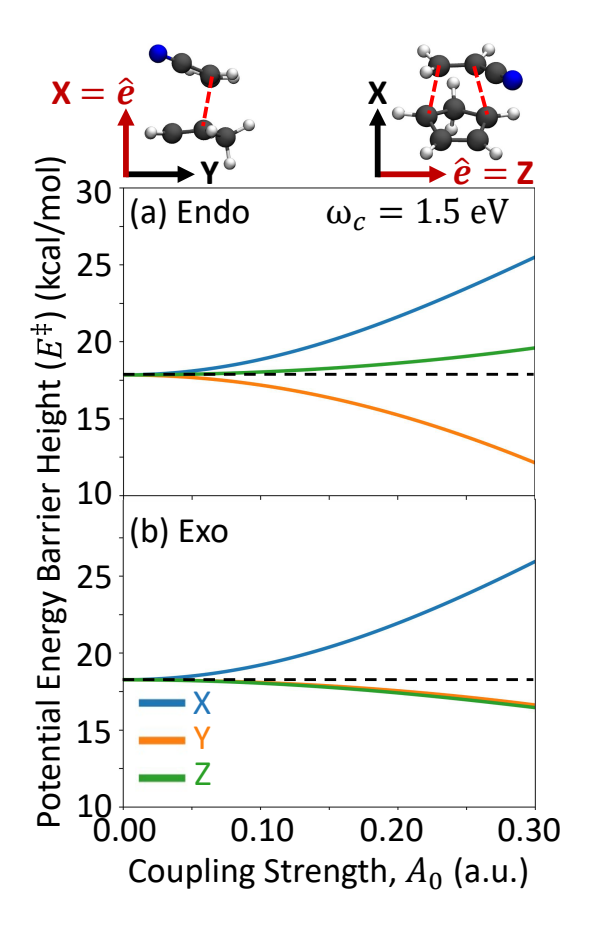


Figure 1: The polaritonic ground state activation energy, defined as the energy difference between the transition state and the reactant geometries, $E^{\ddagger} = E_0(\mathbf{R}_{TS}) - E_0(\mathbf{R}_{reac})$, for the two reaction pathways, (a) Endo and (b) Exo. Here, $E_0(\mathbf{R})$ is the polaritonic ground state energy defined in Eq. 3 at nuclear geometry \mathbf{R} . The colors correspond to cavity polarizations along the X- (blue), Y- (orange), and Z-directions (green). The cavity frequency is $\omega_c = 1.5$ eV. The horizontal dashed line indicates the uncoupled barrier height (i.e., $A_0 = 0.0$ a.u.).

two isomers. In contrast, the Y-direction shows a decrease in both the Endo (5.3 kcal/mol) and the Exo (1.3 kcal/mol) pathways. The Endo isomer exhibits an additional 3.0 kcal/mol reduction in the TS barrier compared to the Exo isomer, thus offering a significant selectivity toward the Endo isomer. The Z-direction also offers a cavity-mediated selectivity, now favoring the Exo isomer. In this case, the Endo isomer's TS barrier is increased by 1.5 kcal/mol, while the Exo barrier height is decreased by 1.8 kcal/mol, generating a 3.3 kcal/mol difference in TS barrier height between isomers. In the Y- and Z-polarization cases, we expect the Endo product yields to be $\mathcal{P}_{\rm Endo} = \exp[-E_{\rm Endo}^{\dagger}/k_{\rm B}T]/\mathcal{Z} = 99.9\%$ and 0.4%, respectively, where $\mathcal{Z} = 99.9\%$

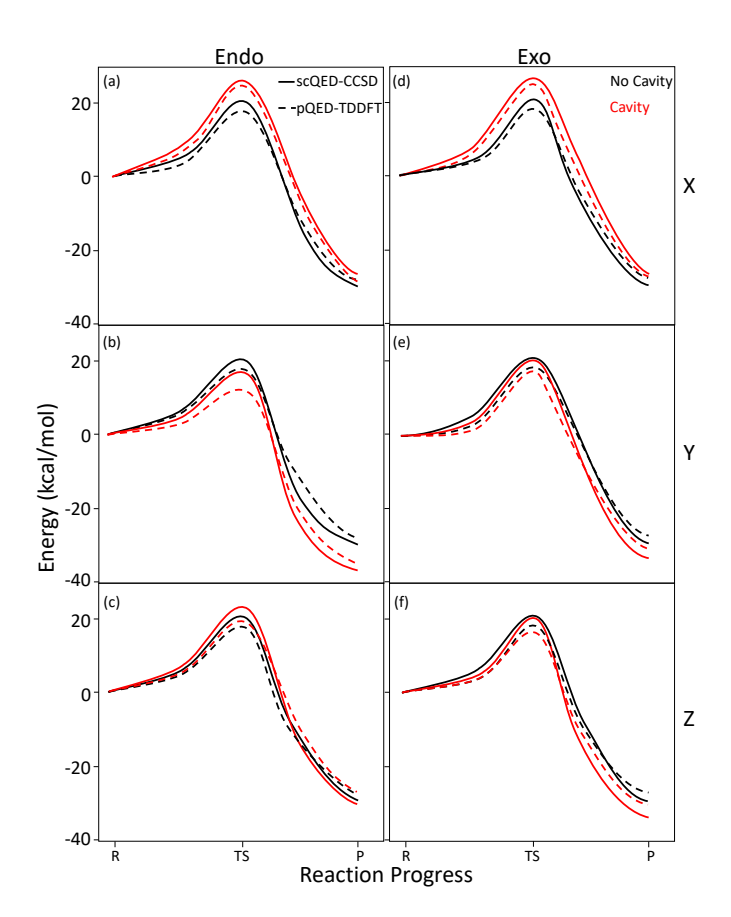


Figure 2: Potential energy surfaces, $E_0(\mathbf{R})$, as functions of the reaction progress from the reactant (R) to the transition state (TS) and to the product (P), inside (red) and outside (black) the cavity for both reaction pathways (a-c) Endo and (d-f) Exo. The (a,d) X, (b,e) Y, and (c,f) Z polarizations of the cavity are shown. The (dashed) pQED-TDDFT approach of the current work is directly compared to the (solid) scQED-CCSD method of Ref. 4. The curves were interpolated between the R, TS, and P data points using a spline approach to improve visual clarity. The light-matter coupling strength is $A_0 = 0.3$ a.u. with cavity frequency $\omega_c = 1.5$ eV.

 $\exp[-E_{\rm Endo}^{\ddagger}/k_{\rm B}T] + \exp[-E_{\rm Exo}^{\ddagger}/k_{\rm B}T]$. Thus, the theoretical results demonstrate that the cavity can offer a novel approach toward the selective isomerization of this DA reaction.

Fig. 2 presents a direct comparison between the pQED-TDDFT of the current work using pQED-TDDFT and that of the high-level scQED-CCSD of Ref. 4 Here, the solid lines represent results obtained from scQED-CCSD, and the dashed lines represent the results from our pQED-TDDFT approach. Note that there are only three data points for each curve, reporting relative energies for reactant (R), transition state (TS), and product (P), and the curves are interpolations (with

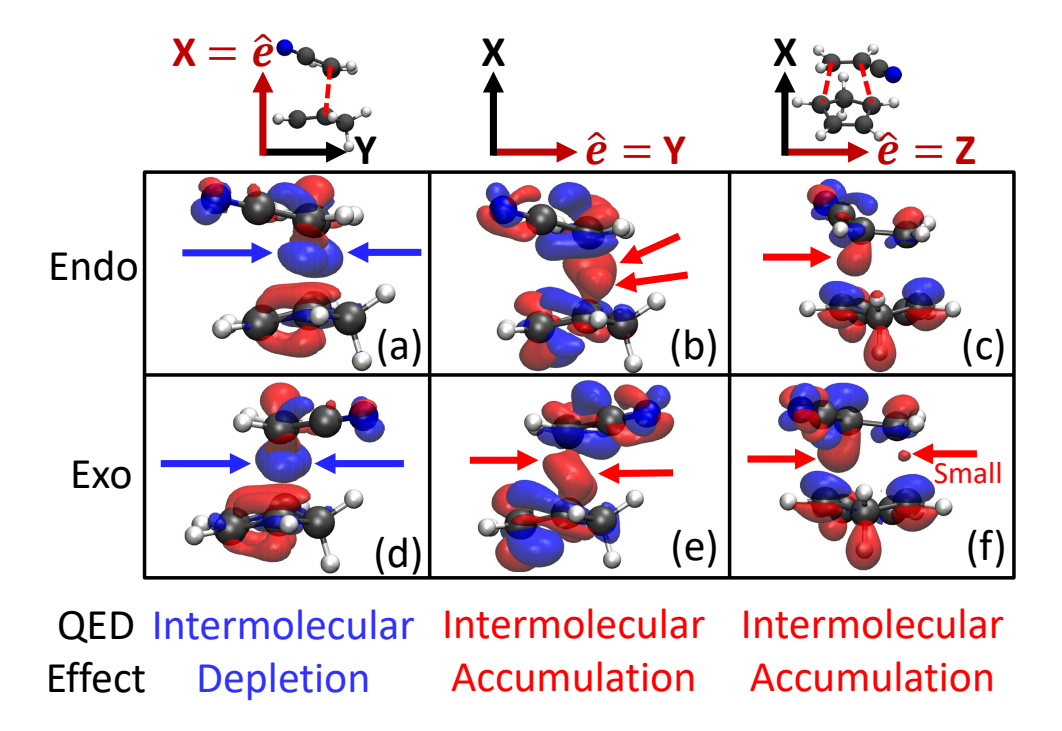


Figure 3: Difference density isosurfaces of the transition state geometries for the (a-c) Endo and (d-f) Exo pathways. The cavity polarization direction is along the (a, d) X-, (b, e) Y-, and (c, f) Z-directions. The isosurfaces in each panel correspond to the difference density, $\Delta \rho_{00}(x,y,z) = \rho_{00}^{\rm M}(x,y,z) - \xi_{00}(x,y,z)$, at the transition state geometry using the pQED-TDDFT approach of the current work. The color indicates the accumulation (red) or depletion (blue) of electron density upon coupling to the cavity. The arrows indicate the corresponding change of electron density that can be interpreted as "intermolecular bonding orbitals". In all cases, the light-matter coupling strength $A_0 = 0.2$ a.u. with cavity frequency $\omega_c = 1.5$ eV. The isovalue chosen for the X-direction is 1.0 m|e|/ \mathring{A}^2 and 0.2 m|e|/ \mathring{A}^2 for the Y- and Z-polariations, where m|e| = |e|×1000 and |e| is the charge of an electron.

an interpolated spline grid portraying the rest of the potential energy surface) that provide visual guidance. Black curves represent the case outside the cavity, and the red curves represent the case inside the cavity. Overall, our pQED results agree semi-quantitatively with the accurate and expensive scQED-CCSD, in terms of predicting the relative trend of barrier modifications for inside and outside the cavity cases. In general, we find only minor quantitative differences between the two approaches that can be rationalized by the known deviations between standard CCSD and DFT methodologies, which are expected to reach 1-5 kcal/mol. Here, such deviations reach up to 3.0 kcal/mol for the Endo pathway and 2.6 kcal/mol for the Exo pathway, signifying that our pQED-TDDFT is well within the expected error of the bare many-body approach itself. More importantly, our pQED-TDDFT results portray the same semi-quantitative behavior of the Endo and Exo potential energy surfaces as the scQED-CCSD for all data points except two: the X- and Z-polarization directions for the Endo

product energies. In the X-polarization direction, the scQED-CCSD approach predicts an increase in energy for the Endo product, while our pQED-TDDFT method indicates a slight decrease. In the Z-polarization direction, the scQED-CCSD results show a minor decrease in product energy, whereas the pQED-TDDFT approach shows an increase. A more detailed analysis of these subtle differences is available in the Supporting Information. Furthermore, the differences in the QED-CCSD and pQED-TDDFT energies are less than 2 kcal/mol and well within the error expected between the standard TDDFT and CCSD methodologies and thus acceptable for our qualitative exploration of this DA reaction which, for the rest of the work, only focuses on the correctly reproduced TS barrier geometries/energies.

To rationalize the observations seen in Fig. 1 and Fig. 2 (which was not presented in the earlier work of Ref. 4), Fig. 3 shows the density difference isosurfaces^{6,7} for the TS geometries for the Endo (top) and Exo (bottom) isomers for all three principle cavity polariation directions: x (left), Y

(middle), and Z (right). The difference density function is defined as $\Delta \rho_{00}(\mathbf{r}) = \rho_{00}^{\mathrm{M}}(\mathbf{r}) - \xi_{00}(\mathbf{r}),$ where $\rho_{00}^{M} = \text{Tr}_{ph}[\hat{\rho}_{00}] = \text{Tr}_{ph}[|\Phi_{0}\rangle\langle\Phi_{0}|]$ is the total ground state polaritonic density with the photon DOFs traced out. $\xi_{00}(\mathbf{r}) = \psi_0^*(\mathbf{r})\psi_0(\mathbf{r})$ is the bare electronic ground state density. The difference between these two densities portrays the effects of cavity-induced electronic redistribution around the molecule. The regions in which $\Delta \rho_{00}(\mathbf{r}) > 0$ (red colored) indicate that a gain of electron density has occurred and depletion when $\Delta \rho_{00}(\mathbf{r}) < 0$ (blue colored). Additional visualization angles are shown in Fig. S4 in the **Supporting Information**. This effect can be rationalized via chemical intuition by considering that the cavity can induce redistribution (exchange of character) between bare occupied and unoccupied single-particle orbitals (e.g., $HOMO \leftrightarrow LUMO$), which allows for changes to the standard molecular orbital theory inside the cavity. 10

The X-polarization direction showcased a simultaneous increase in TS barrier energy for the Endo and Exo isomers (see Fig. 1), thus, we expect that the potential chemical bond between the two reactant molecules is weakened by the presence of the cavity for both isomer configurations. Fig. 3a,d show the ground state difference density isosurface for the Endo (Fig. 3a) and Exo (Fig. 3d) isomers with the cavity polarized along the X-direction of the molecule (see cartesian axes above Fig. 3a). The region between the reactant molecules is blue, which indicates that this region has been depleted of electron density. This region is also responsible for the formation of the intermolecular bond during the reaction. Since this region has lost these intermolecular bonding electrons, the TS geometry has been destabilized compared to outside the cavity. Contrary to this result, the Y-polarization of the cavity induced a stabilization of the TS barrier energy (Fig. 1). Fig. 3b,e show the difference density in this case, and, opposite to Fig. 3a,d, we find an increase in electron density in the region between the reactant species, this strengthening the intermolecular bond at the TS geometry and reducing the TS barrier energy.

The regions not localized between the reactant species in Fig. 3 are considered as intra-molecular density redistributions. These density differences have a similar shape as intramolecular π -bonding orbitals. This is especially evident in the cyclopentadiene molecule. For the X-polarization, these or-

bitals exhibit electron density accumulation from the intermolecular bonding orbitals. For the Y-polarization, on the other hand, these intramolecular π -bonding orbitals donate their electrons to the intermolecular bond. Thus, the effects of the cavity are to induce changes to the bonding structure of the reactant species, thus either enhancing or weakening the bond formation depending on the cavity polarization direction.

The Z-polarization direction is weakly changing the TS barrier energy (Fig. 1) and oppositely between the Endo and Exo isomers. Notably, the difference density in this case (Fig. 3c,f) exhibits weaker and asymmetric changes to the intermolecular region. Note that the molecule is rotated by 90 degrees about the X-axis in Fig. 3c,f compared to Fig. 3a,b,d,e for visual clarity. Additionally, the intramolecular density, especially on the bottom molecule of the figure (cyclopentadiene) shows a different symmetry compared to those shown in Fig. 3a,b,d,e where the underside of the intramolecular π -bonds are accumulating electron density while the top side is being depleted. Overall, the redistribution of electron density does not facilitate the formation of the two covalent bonds and thus showcases a weaker change to the TS barrier height compared to the X- and Y-polarization directions.

Overall, we have used the difference density function to develop a chemically appealing interpretation of the cavity-modified DA reaction between cyclopentadiene and acrylonitrile. In particular, the cavity-mediated redistribution of charges closely resembles the inter- and intramolecular bonding orbitals. The electron density is explicitly modified by the cavity to facilitate the intermolecular bonds by donating electron density from intramolecular π -orbitals (largely localized on the cyclopentadiene species) to the forming intermolecular bond. The intermolecular bonds can instead be weakened by the interactions with the cavity by removing electron density from the intermolecular bonds and donating it to the intramolecular bonds.

The cavity polarization directions along the principal cartesian axes (X, Y, and Z) were taken as a benchmark from the previous work of Ref. 4. However, the use of these cartesian directions as "important" field polarization directions is a theoretical choice and may be difficult to control in experiments, despite the exciting progress on using super-molecular host-guest chemistry when cou-

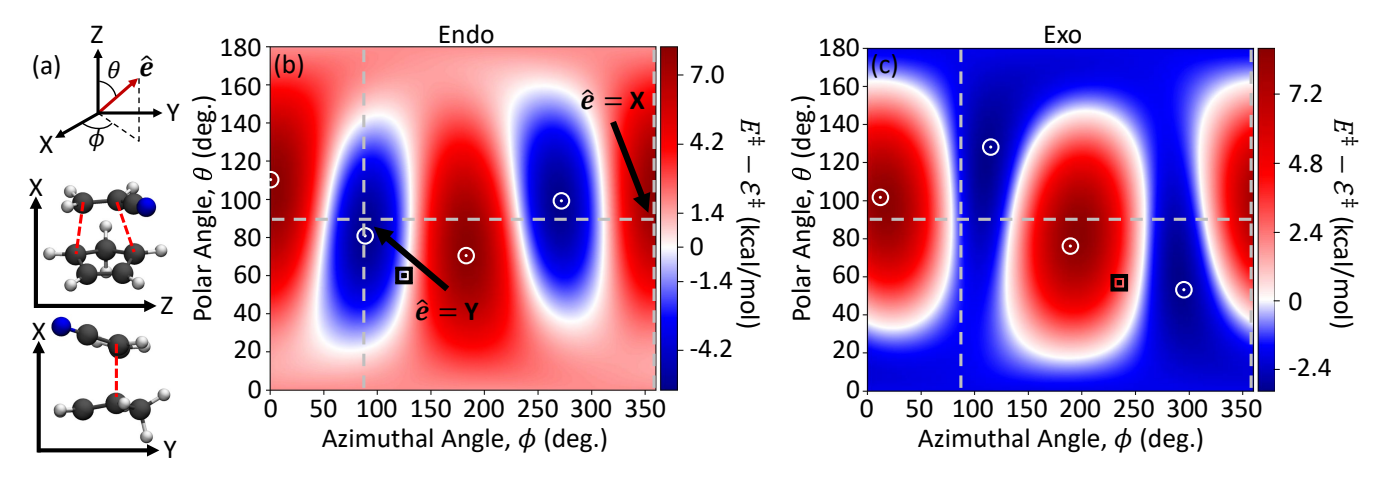


Figure 4: (a) Schematic illustration of the spherical coordinate system with an arbitrary cavity polarization vector $\hat{e}(\phi,\theta)$ and two orientations of the molecule with respect to the primary cartesian axes. (b,c) The difference between the polaritonic transition state barrier, $E^{\ddagger} = E_0(\mathbf{R}_{TS}) - E_0(\mathbf{R}_{reac})$, and the barrier of the bare molecular system, $\mathcal{E}^{\ddagger} = \mathcal{E}_0(\mathbf{R}_{TS}) - \mathcal{E}_0(\mathbf{R}_{reac})$, for the (b) Endo and (c) Exo reaction pathways as functions of the azimuthal ϕ and polar θ angles. The color bar indicates the sign and magnitude of the difference of the energy barrier height, $E^{\ddagger} - \mathcal{E}^{\ddagger}$. The blue regions indicate where the transition state barrier is lowered compared to outside the cavity. The white symbols indicate the maxima and minima values, with only two non-degenerate points on each pathway and are related to the other set by symmetry. For both panels, the light-matter coupling strength $A_0 = 0.3$ a.u. and cavity frequency $\omega_c = 1.5$ eV.

pling a single molecule with the plasmonic cavity. ³³ With this in mind, we explore an arbitrary cavity field polarization vector $\hat{e} = \hat{e}(\phi, \theta)$, where ϕ and θ are the azimuthal and polar angles, respectively, defined schematically in Fig. 4a. Fig. 4b and Fig. 4c show the change in TS barrier energy $\Delta E^{\ddagger}(\phi,\theta) = E^{\ddagger}(\phi,\theta) - \mathcal{E}^{\ddagger}$ for the Endo and Exo isomer, respectively, with light-matter coupling strength $A_0 = 0.3$ a.u. and cavity frequency $\omega_{\rm c} = 1.5$ eV. Here, $E^{\ddagger}(\phi, \theta)$ is the polaritonic ground state TS barrier energy and \mathcal{E}_0 is the bare electronic ground state TS barrier energy (equivalent to E^{\ddagger} with $A_0 = 0.0$ a.u. and $\omega_c = 0.0$ eV). The negative regions indicate a reduction in the TS barrier height inside the cavity, while the red regions show an increase to the TS barrier height.

In Fig. 4b, the Endo isomer at certain values of (ϕ, θ) has a TS barrier energy that is maximized (white circle in the red region) and minimized (white circle in the blue region) for this choice of cavity parameters. We define these special configuration points as $(\phi_1, \theta_1) = (3.3^{\circ}, 111.2^{\circ})$ and $(\phi_2, \theta_2) = (91.7^{\circ}, 80.2^{\circ})$, respectively. Connecting to the previous figures, the X- and Y-directions are equivalent to $(\phi, \theta) = (0^{\circ}, 90^{\circ}) = (360^{\circ}, 90^{\circ})$ and $(\phi, \theta) = (90^{\circ}, 90^{\circ}) = (270^{\circ}, 90^{\circ})$, respectively. In the Endo case (Fig. 4b), the X- and Y-polarization directions are near to the critical points (ϕ_1, θ_1) and (ϕ_2, θ_2) . However, for the

Exo isomer (Fig. 4c), the critical points are located at $(\phi_3, \theta_3) = (11.5^{\circ}, 103.1^{\circ})$ and $(\phi_4, \theta_4) =$ $(114.6^{\circ}, 126.1^{\circ})$. Hence, the Y-axis direction is far from either of the extrema for the Exo case. In fact, the Y-direction lies on the border between the stabilizing region (blue) and the destabilizing region (red). In both cases, the Z-direction is far from any critical point, implying that this direction of cavity polarization is not optimal in either isomer. Later, in Fig. 7, the Z-polarization is shown to still be valuable in cavity-induced selectivity even though both isomers, individually, experience a mediocre cavity effect. We found the maximum and minimum critical points for the Endo pathway to be $(\phi_1, \theta_1) = (\phi_{\text{MAX}}^{\text{Endo}}, \theta_{\text{MAX}}^{\text{Endo}}) = (3.3^{\circ}, 111.2^{\circ})$ and $(\phi_2, \theta_2) = (\phi_{\text{MIN}}^{\text{Endo}}, \theta_{\text{MIN}}^{\text{Endo}}) = (91.7^{\circ}, 80.2^{\circ}); \text{ for Exo}$ pathway, the points are $(\phi_3, \theta_3) = (\phi_{\text{MAX}}^{\text{Exo}}, \theta_{\text{MAX}}^{\text{Exo}}) = (11.5^{\circ}, 103.1^{\circ})$ and $(\phi_4, \theta_4) = (\phi_{\text{MIN}}^{\text{Exo}}, \theta_{\text{MIN}}^{\text{Exo}}) = (0.5 \text{ mag})$ (114.6°, 126.1°), respectively. The black square symbols indicate the ground state dipole moment unit vectors, $\vec{\mu}_{00}$, for the Endo and Exo pathways, which are (Fig. 4b) $(125.6^{\circ}, 60.8^{\circ})$ and (Fig. 4c) $(235.7^{\circ}, 56.9^{\circ})$, respectively.

Fig. 5 shows the TS barrier energy E^{\ddagger} as a function of the light-matter coupling strength A_0 for the above-mentioned critical angles for the cavity polarization vector (ϕ_i, θ_i) for both isomers. The cavity frequency is $\omega_c = 1.5$ eV. It is evident that

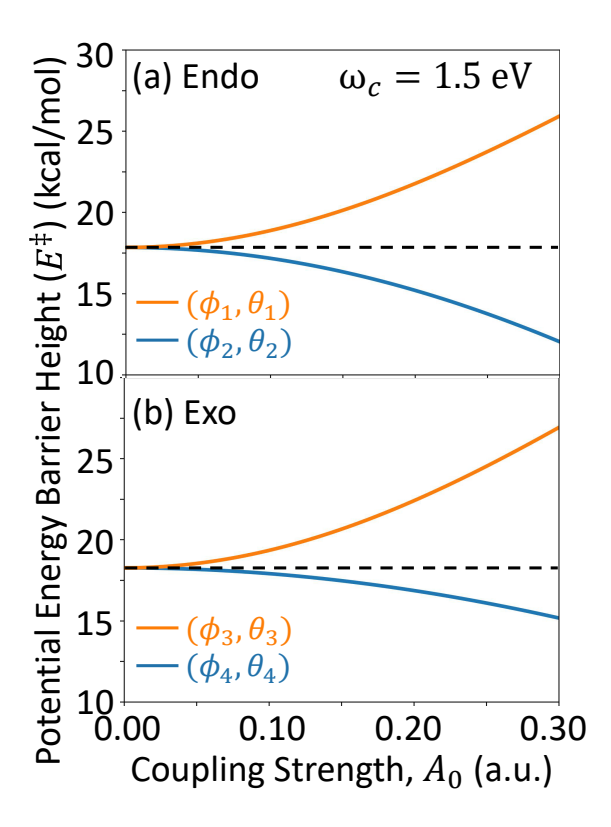


Figure 5: The polaritonic ground state activation energy, defined as the energy difference between the transition state and the reactant geometries, $E^{\ddagger} = E_0(\mathbf{R}_{TS}) - E_0(\mathbf{R}_{reac})$, for the two reaction pathways, (a) Endo and (b) Exo. The cavity polarizations are shown at the critical points for each pathway: (ϕ_1, θ_1) and (ϕ_3, θ_3) (MAX in orange); (ϕ_2, θ_2) and (ϕ_4, θ_4) (MIN in blue). The cavity frequency is $\omega_c = 1.5$ eV. The horizontal dashed line indicates the uncoupled barrier height (i.e., $A_0 = 0.0$ a.u.).

the (ϕ_1, θ_1) and (ϕ_3, θ_3) maximize the individual isomer TS barrier energies while the (ϕ_2, θ_2) and (ϕ_4, θ_4) minimize this energy for all values of coupling strength A_0 . In turn, we can inspect the ground state difference density isosurfaces for these critical points, as shown in Fig. 6. As expected, the polarization angles that maximize the TS barrier energy contain intermolecular electron density depletion, destabilizing the forming bond, as well as electron accumulation in the intramolecular bonding π -orbitals of each reactant molecule. The opposite is again true for the angles that minimize the TS barrier energy, showing electron density accumulation in the intermolecular bonding region. Notably, the intramolecular π -bonding orbitals showcase asymmetric accumulation/depletion, similar to the Z-polarization in Fig. 3c,f. We hypothesize that these critical angles of the field induce a

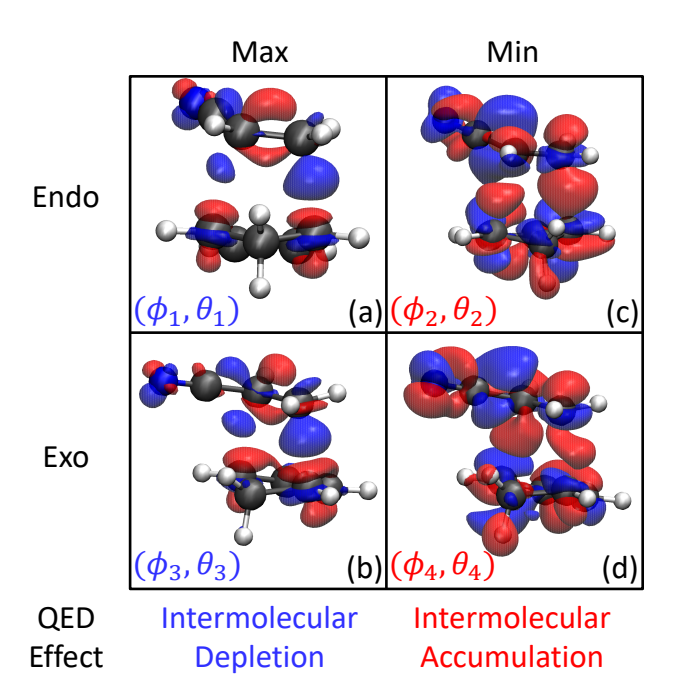


Figure 6: Difference density isosurfaces at the transition state geometries for the (top) Endo and (bottom) Exo pathways. The cavity polarizations are shown at the critical points for each pathway: (a) MAX, Endo pathway (ϕ_1, θ_1); (b) MAX, Exo pathway (ϕ_3, θ_3); (c) MIN, Endo pathway (ϕ_2, θ_2); (d) MIN, Exo pathway (ϕ_4, θ_4). The color indicates the accumulation (red) or depletion (blue) of electron density upon insertion into the cavity. The arrows indicate the intermolecular bonding orbitals. In all cases, the light-matter coupling strength $A_0 = 0.2$ a.u. with cavity frequency $\omega_c = 1.5$ eV. The isovalue chosen for both maxima is $1.0 \text{ m}|e|/\mathring{A}^2$ and $0.2 \text{ m}|e|/\mathring{A}^2$ for the minima, where $\text{m}|e| = |e| \times 1000$ and |e| is the charge of an electron.

complicated redistribution of electron density, not only from the reactant species to the forming intermolecular bond, but also among themselves in a way that further decreases the energy of the TS geometry. Hence, examining only the principle directions X, Y, and Z as defined by chemical intuition will mostly likely not showcase the maximal effects of the complicated electron-photon correlation (as the black square symbols shown in Fig. 4) since the direction of the many coupled permanent and transition dipole matrix elements in the adiabatic electronic basis is not straightforward and likely does not relate to a simple and meaningful chemical property.

Fig. 7a presents the TS barrier energy difference, $E_{\rm Endo}^{\ddagger} - E_{\rm Exo}^{\ddagger}$, as a function of the cavity polarization direction (ϕ, θ) for a fixed cavity frequency

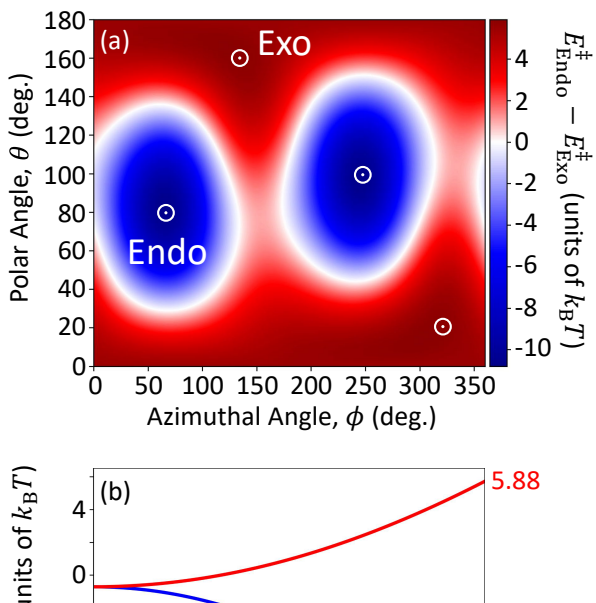


Figure 7: (a) TS energy difference between the Endo and Exo isomers, $E_{\rm Endo}^{\ddagger} - E_{\rm Exo}^{\ddagger}$, as a function of the cavity polarization direction, (ϕ,θ) . The blue region $(E_{\rm Endo}^{\ddagger} < E_{\rm Exo}^{\ddagger})$ indicates that the Endo pathway has a lower barrier energy and is preferable compared to the Exo pathway; the red region, in contrast, indicates that the Exo pathway is preferable. The light-matter coupling strength $A_0 = 0.3$ a.u. and the cavity frequency $\omega_{\rm c} = 1.5$ eV. The white circle-dot symbols indicate the critical points at which $E_{\rm Endo}^{\ddagger} - \tilde{E}_{\rm Exo}^{\ddagger}$ is maximized, $(\phi_{\rm Exo}, \theta_{\rm Exo}) = (137.5^{\circ}, 160.4^{\circ})$, or minimized, $(\phi_{\rm Endo}, \theta_{\rm Endo}) = (68.8^{\circ}, 80.2^{\circ}),$ offering the maximum amount of selectiveity for the Exo and Endo isomers, respectively. (b) TS barrier energy difference between the Endo and Exo isomers, $E_{\rm Endo}^{\ddagger} - E_{\rm Exo}^{\ddagger}$ as a function of the light-matter coupling strength at the critical angles which produce the maximal selectivity of Endo (blue) and Exo (red) isomers.

 $\omega_{\rm c}=1.5$ eV and light-matter coupling strength $A_0=0.3$ a.u. This figure depicts the energy difference between the barrier heights of the two isomers, $E_{\rm Endo}^{\dagger}-E_{\rm Exo}^{\dagger}$. Thus, Fig. 7 is related to the probability of forming either Endo or Exo species at a given orientation of the molecule with respect to the cavity field direction. Negative values of this quantity (blue regions) indicate parameter regimes where the Endo pathway is lower in TS energy compared to the Exo pathway. Contrary to this, posi-

tive values indicate regions where the Exo pathway TS has a lower energy. The cavity polarization angles at which the highest amount of selectivity toward the Endo, $(\phi_{\rm Endo}, \theta_{\rm Endo}) = (68.8^{\circ}, 80.2^{\circ})$ at 5.88 k_BT, and Exo, $(\phi_{\rm Exo}, \theta_{\rm Exo}) = (137.5^{\circ}, 160.4^{\circ})$ at -10.73 k_BT are the critical points. These angles are shown as white circle-dots in Fig. 7a.

In experiments, control over the light-matter coupling strength A_0 is difficult and is often susceptible to many environmental factors. While our calculations predict strong selectivity at these critical angles of cavity polarization direction, the selectivity at weaker light-matter coupling strengths A_0 may provide a deeper insight into experimental observations. Fig. 7b presents the TS barrier energy difference, $E_{\rm Endo}^{\ddagger} - E_{\rm Exo}^{\ddagger}$, as a function of the lightmatter coupling strength A_0 for both of the critical angles shown in Fig. 7a. At small values of lightmatter coupling ($A_0 < 0.05$ a.u.), negligible selectivity change is predicted. Our calculations predict that, at these critical angles, prominent Endo selectivity can be achieved at or above $A_0 = 0.10$ a.u. at which the TS barrier energy difference is greater than $2 k_{\rm B}T$ at room temperature. For the Exo isomer, the selectivity is weaker and requires at least $A_0 = 0.20$ a.u. for the same degree of selectivity induced by the TS barrier energy difference. Hence, in the experiment, strong selectivity in the reaction is already achievable with current plasmonic cavity designs. 23,24

Furthermore, while experimentally feasible, ³³ it is often difficult to control the orientation of the molecules with respect to the cavity's electric field polarization (ϕ, θ) . In the experiment, we expect a random orientation of the molecules (isotropic disorder). We calculate the angular average of a cavity modified observable $O(\phi, \theta)$ as follows

$$\langle O(\phi, \theta) \rangle = \frac{\int \sin \theta d\theta \int d\phi O(\phi, \theta)}{\int \sin \theta d\theta \int d\phi}.$$
 (5)

For example, the average transition state energy difference between the Endo and Exo isomers is $\langle E_{\rm Endo}^{\ddagger} - E_{\rm Exo}^{\ddagger} \rangle = -0.9212k_{\rm B}T$ at room temperature (300 K) using data in Fig. 7a. This implies that, even by considering the isotropic disorder, the Endo pathway is still preferred by nearly one $k_{\rm B}T$ at room temperature, whereas for outside the cavity case, there should be an equal mixture of the Endo and Exo products. Hence, we have theoretically shown that this DA reaction will provide appreciable selectivity inside the cavity, even if the

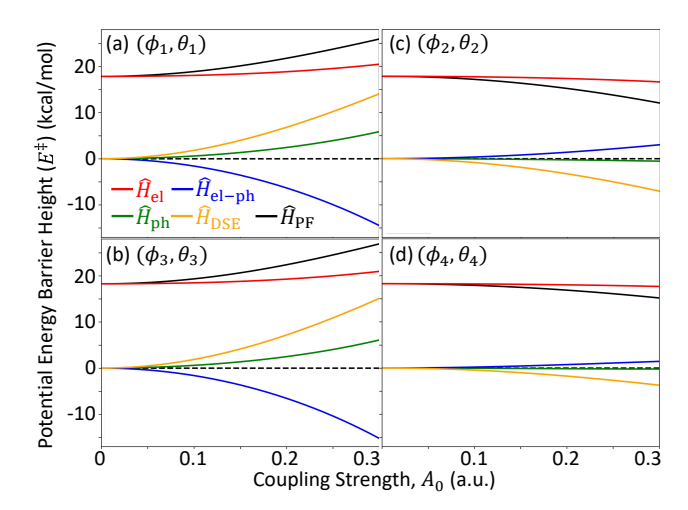


Figure 8: Energy contributions from individual terms from \hat{H}_{PF} in Eq. 1 to the ground state energy barrier height. Components are \hat{H}_{el} in red, \hat{H}_{el-ph} in blue, \hat{H}_{ph} in green and \hat{H}_{DSE} in gold. The horizontal dashed line indicates the barrier height changes outside the cavity (i.e., $A_0 = 0.0$ a.u.). The cavity frequency is $\omega_c = 1.5$ eV.

orientation of the molecules cannot be controlled.

Finally, we investigate the individual contributions to the cavity-induced selectivity of this DA reaction. Fig. 8 presents the contributions from individual terms in Eq. 1 to the TS energies at the critical cavity polarization angles for the Endo (Fig. 8a,c) and Exo (Fig. 8b,d) isomers. The energy contributions are calculated as $E_a^{\dagger} = \langle \Phi_0(\mathbf{R}_{TS}) | \hat{H}_a | \Phi_0(\mathbf{R}_{TS}) \rangle - \langle \Phi_0(\mathbf{R}_{reac}) | \hat{H}_a | \Phi_0(\mathbf{R}_{reac}) \rangle$, where $\hat{H}_a \in \{\hat{H}_{PF}, \hat{H}_{el}, \hat{H}_{ph}, \hat{H}_{el-ph}, \hat{H}_{DSE}\}$. Further,

 $\hat{H}_a \in \{\hat{H}_{\mathrm{PF}}, \hat{H}_{\mathrm{el}}, \hat{H}_{\mathrm{ph}}, \hat{H}_{\mathrm{el-ph}}, \hat{H}_{\mathrm{DSE}}\}$. Further, $|\Phi_0(\mathbf{R})\rangle$ is the ground state polaritonic wavefunction, always defined by the total PF Hamiltonian $\hat{H}_{\mathrm{PF}}|\Phi_0(\mathbf{R})\rangle = E_0(\mathbf{R})|\Phi_0(\mathbf{R})\rangle$ (Eq. 3). These contributions are shown for each of the four cavity polarization directions defined in Fig. 4: (ϕ_1, θ_1) in Fig. 8a, (ϕ_3, θ_3) in Fig. 8b, (ϕ_2, θ_2) in Fig. 8c, and (ϕ_4, θ_4) in Fig. 8d. These angles represent the largest increase (Fig. 8a,b) and largest decrease (Fig. 8c,d) in the transition state energy for the Endo (Fig. 8a,c) and Exo (Fig. 8b,d) configurations. The cavity frequency is set to be $\omega_c = 1.5$ eV. In the **Supporting Information**, Fig. S5 and Fig. S6 present the same data but for the reactant and TS geometries, individually.

By construction, the total energy \hat{H}_{PF} (solid black curve) for (ϕ_1, θ_1) and (ϕ_3, θ_3) increases as a function of the light-matter coupling strength and decreases for (ϕ_2, θ_2) and (ϕ_4, θ_4) . Of most importance and interest are the two interaction

terms $\hat{H}_{\rm el-ph}$ (solid red curve) and $\hat{H}_{\rm DSE}$ (solid gold curve), which are responsible for the modifications to the TS barrier energy E^{\ddagger} inside the cavity. For both critical angles at which the TS barrier energy is maximized (Fig. 8a,b), the DSE contributes positively to the energy while the direct electron-photon interaction provides a negative contribution. Note that the energy of the DSE for a single-molecule coupled to a cavity is a positive contribution while the direct interaction term is negative. Here, we are showing the energy difference between two nuclear geometries, $E^{\ddagger} = E_{TS} - E_{reac}$, for which the contribution of either term can be positive or negative (see Fig. S5 and Fig. S6 in the **Supporting Information** for the absolute energies of each term). For the critical angles in which the TS barrier energy is minimized (Fig. 8c,d), the opposite trends are observed, where the DSE contributes negatively while the direct interaction term is positive. Additionally, the magnitudes of all terms are reduced since the cavityinduces TS barrier decreases (negative values/blue in Fig. 4) are less in magnitude than the cavityinduced increases (positive values/red in Fig. 4). From Fig. 8, it is clear that the DSE is directly related to the chemically relevant modifications to the ground state energies, since the DSE contribution nearly quantitatively reproduces the changes to the TS barrier energy in all cases (i.e., other contributions largely cancel among each other). This also provides confirmation of the various mean-field QED-HF calculations 7,10,18,19,21,21,22,34 as well as high-level approaches $^{4,7-9,14,15,17,20,35-39}$ in the community exploring ground state cavitymodifications. 5,6,13,16,25-28

Conclusions

We theoretically investigated the cavity modification on a textbook ground state Diels-Alder (DA) reaction. By coupling to a quantized cavity radiation field, one can selectively generate one type of the product (Endo or Exo) compared to the outside the cavity case (under standard reaction conditions) where the reaction produces an equal mixture of both products. Our results demonstrate that the cavity induces selectivity toward the Endo isomer, even for moderate coupling strength, as well as for random molecular orientations (isotropi-

cal disorders). In addition, we have shown that the pQED-TDDFT method semi-quantitatively agrees with the high-level scQED-CCSD approach ⁴ and with errors between the two approaches less than 3 kcal/mol.

By computing the ground state difference density, we show that the cavity induces a redistribution of electron density to stabilize or destabilize the TS geometry, depending on the cavity polarization direction. Cavity-induced stabilization occurs by shifting electron density from intramolecular π -bonding orbitals to intermolecular bonding orbitals. Destabilization occurs through the opposite mechanism, where the intermolecular bonding orbitals donate their electron density to intramolecular π -bonding orbitals. Our results have provided chemically relevant insights into the cavity-induced changes to the ground state chemistry and, thus, changes to the molecular orbital theory inside the cavity. ¹⁰

We further explore an arbitrary molecular orientation relative to the cavity polarization direction, which leads to critical polarization angles that maximize the Endo or Exo-selectivity of the reaction. Here, we show that the optimal selectivity for the ground state reaction, in terms of the cavity polarization direction, does not correspond to a simple chemically relevant direction but involves a complicated interplay between the many permanent and transition dipole orientations of the reacting molecules. Overall, we show that maximum selectivity for the Endo and Exo isomers can be achieved with relative barrier energies approaching ~ 5 and $\sim 10k_{\rm B}T$, respectively. When assuming the isotropic disorder in the orientation of the molecule with respect to the cavity polarization direction, we find that the Endo isomer is preferred by $\sim k_{\rm B}T$, which is still significantly different than the situation outside the cavity.

Finally, we decompose the individual energy contributions from the PF Hamiltonian (in Eq. 1) and provide a discussion on the effects of the dipole self-energy on the polaritonic ground state. The DSE contribution to the TS barrier energy has identical trends with the energy of the total Hamiltonian. Thus, we conclude that the DSE is the leading order physics to the cavity-mediated ground state modifications in this particular DA reaction, which is in agreement with many other works at the mean-field QED-HF level and beyond. We hope this work enables further study of ground state

chemistry inside the cavity that includes (i) identification of the optimal cavity polarization direction for each reaction (ii) a quantitative benchmark against other approaches, and (iii) a detailed comparison of the cavity parameters with state-of-theart experimental cavity designs.

Acknowledgement This work was supported by the Air Force Office of Scientific Research under AFOSR Award No. FA9550-23-1-0438. The software development for molecular polariton calculations in this work was partially supported by the National Science Foundation's Office of Advanced Cyberinfrastructure under Award No. OAC-2311442. B.M.W. was partially supported by the National Science Foundation under grant number CHE-2124398 during the early stage of the project. Part of this work is based on the undergraduate thesis of J. W. The software development in this work was supported by the National Science Foundation's Office of Advanced Cyber-infrastructure under Award No. OAC2311442. P.H. appreciates the support of the Cottrell Scholar Award (a program by the Research Corporation for Science Advancement). Computing resources were provided by the Center for Integrated Research Computing (CIRC) at the University of Rochester. P.H. appreciates the valuable discussions with Todd Krauss and Joe Dinnocenzo.

Supporting Information Available

Additional figures that support the discussion in the main text are provided, namely, light-matter coupling strength scans, pQED-TDDFT/scQED-CCSD benchmark comparisons, three-dimensional isosurfaces of the difference density, and energy contributions of reactant and transition state geometries.

References

- (1) Anslyn, E. V.; Dougherty, D. A. *Modern Physical Organic Chemistry*; University Science Books, 2006.
- (2) Loudon, M.; Parise, J. Organic Chemistry; Macmillan Learning, 2015.

- (3) Woodward, R. B.; Hoffmann, R. Stereochemistry of Electrocyclic Reactions. *J. Am. Chem. Soc.* **1965**, *87*, 395–397.
- (4) Pavošević, F.; Smith, R. L.; Rubio, A. Computational study on the catalytic control of endo/exo Diels-Alder reactions by cavity quantum vacuum fluctuations. *Nat Commun* **2023**, *14*, 2766.
- (5) Weight, B. M.; Krauss, T. D.; Huo, P. Investigating Molecular Exciton Polaritons Using Ab Initio Cavity Quantum Electrodynamics. J. Phys. Chem. Lett. 2023, 14, 5901–5913.
- (6) Weight, B. M.; Weix, D. J.; Tonzetich, Z. J.; Krauss, T. D.; Huo, P. Cavity Quantum Electrodynamics Enables para- and ortho-Selective Electrophilic Bromination of Nitrobenzene. *Journal of the American Chemi*cal Society 2024, 146, 16184–16193.
- (7) Haugland, T. S.; Ronca, E.; Kjønstad, E. F.; Rubio, A.; Koch, H. Coupled Cluster Theory for Molecular Polaritons: Changing Ground and Excited States. *Phys. Rev. X* **2020**, *10*, 041043.
- (8) DePrince, A. E. Cavity-modulated ionization potentials and electron affinities from quantum electrodynamics coupled-cluster theory. *J. Phys. Chem. A* 2022, 126, 49, 9303–9312 **2022**, 154, 094112.
- (9) Weight, B. M.; Tretiak, S.; Zhang, Y. Diffusion quantum Monte Carlo approach to the polaritonic ground state. *Phys. Rev. A* **2024**, 109, 032804.
- (10) Riso, R. R.; Haugland, T. S.; Ronca, E.; Koch, H. Molecular orbital theory in cavity QED environments. *Nat. Commun.* 2022, 13, 1368.
- (11) Mandal, A.; Taylor, M. A. D.; Weight, B. M.; Koessler, E. R.; Li, X.; Huo, P. Theoretical Advances in Polariton Chemistry and Molecular Cavity Quantum Electrodynamics. 2023, 123, 9786–9879.
- (12) Taylor, M. A. D.; Mandal, A.; Zhou, W.; Huo, P. Resolution of Gauge Ambiguities in Molecular Cavity Quantum Electrodynamics. Phys. Rev. Lett. 2020, 125, 123602.

- (13) Mandal, A.; Taylor, M. A. D.; Huo, P. Theory for Cavity-Modified Ground-State Reactivities via Electron-Photon Interactions. J. Phys. Chem. A 2023, 127, 6830-6841.
- (14) Pavošević, F.; Hammes-Schiffer, S.; Rubio, A.; Flick, J. Cavity-Modulated Proton Transfer Reactions. J. Am. Chem. Soc. 2022, 144, 4995–5002.
- (15) Pavosevic, F.; Smith, R. L.; Rubio, A. Cavity-Click Chemistry: Cavity-Catalyzed Azide-Alkyne Cycloaddition. 2023; http://arxiv.org/abs/2305.09496.
- (16) Haugland, T. S.; Philbin, J. P.; Ghosh, T. K.; Chen, M.; Koch, H.; Narang, P. Understanding the polaritonic ground state in cavity quantum electrodynamics. 2023; http://arxiv.org/abs/2307.14822.
- (17) Haugland, T. S.; Schäfer, C.; Ronca, E.; Rubio, A.; Koch, H. Intermolecular interactions in optical cavities: An ab initio QED study. J. Chem. Phys. 2021, 154, 094113.
- (18) Foley, J. J., IV; McTague, J. F.; De-Prince, A. E., III Ab initio methods for polariton chemistry. *Chemical Physics Reviews* **2023**, 4, 041301.
- (19) Weight, B. M.; Li, X.; Zhang, Y. Theory and modeling of light-matter interactions in chemistry: current and future. Phys. Chem. Chem. Phys. 2023,
- (20) DePrince, A. E. Cavity-modulated ionization potentials and electron affinities from quantum electrodynamics coupled-cluster theory. J. Chem. Phys. 2022, 154, 094112.
- (21) Li, X.; Zhang, Y. First-principles molecular quantum electrodynamics theory at all coupling strengths. **2023**, arXiv, 10.48550/arXiv.2310.18228.
- (22) Mazin, I.; Zhang, Y. Light-Matter Hybridization and Entanglement from the First-Principles. **2024**, arXiv, 10.48550/arXiv.2411.15022.
- (23) Akselrod, G. M.; Huang, J.; Hoang, T. B.; Bowen, P. T.; Su, L.; Smith, D. R.; Mikkelsen, M. H. Large-Area Metasurface

- Perfect Absorbers from Visible to Near-Infrared. *Advanced Materials* **2015**, *27*, 8028–8034.
- (24) Hoang, Τ. B.: Akselrod. M.; Mikkelsen, Μ. Η. Ultrafast Room-Single Temperature Photon Emission from Quantum Dots Coupled to Plasmonic NanoLettersNanocavities. 2016, 16, 270-275.
- (25) Flick, J.; Schäfer, C.; Ruggenthaler, M.; Appel, H.; Rubio, A. Ab Initio Optimized Effective Potentials for Real Molecules in Optical Cavities: Photon Contributions to the Molecular Ground State. ACS Photonics 2018, 5, 992–1005.
- (26) Rokaj, V.; Welakuh, D. M.; Ruggenthaler, M.; Rubio, A. Light-matter interaction in the long-wavelength limit: no groundstate without dipole self-energy. J. Phys. B: At. Mol. Opt. Phys. 2018, 51, 034005.
- (27) Schäfer, C.; Ruggenthaler, M.; Rokaj, V.; Rubio, A. Relevance of the Quadratic Diamagnetic and Self-Polarization Terms in Cavity Quantum Electrodynamics. ACS Photonics 2020, 7, 975–990.
- (28) Ruggenthaler, M.; Flick, J.; Pellegrini, C.; Appel, H.; Tokatly, I. V.; Rubio, A. Quantum-electrodynamical density-functional theory: Bridging quantum optics and electronic-structure theory. *Phys. Rev. A* **2014**, *90*, 012508.
- (29) Jaynes, E. T.; Cummings, F. W. Comparison of quantum and semiclassical radiation theories with application to the beam maser. *Proc. IEEE* **1963**, *51*, 89–109.
- (30) Epifanovsky, E. et al. Software for the frontiers of quantum chemistry: An overview of developments in the Q-Chem 5 package. *J. Chem. Phys.* **2021**, *155*, 084801.
- (31) Simpkins, B. S.; Dunkelberger, A. D.; Vurgaftman, I. Control, Modulation, and Analytical Descriptions of Vibrational Strong Coupling. *Chemical Reviews* **0**, θ, null, PMID: 37018158.

- (32) Ebbesen, T. W. Hybrid Light–Matter States in a Molecular and Material Science Perspective. Acc. Chem. Res. 2016, 49, 2403–2412.
- (33) Chikkaraddy, R.; de Nijs, B.; Benz, F.; Barrow, S. J.; Scherman, O. A.; Rosta, E.; Demetriadou, A.; Fox, P.; Hess, O.; Baumberg, J. J. Single-molecule strong coupling at room temperature in plasmonic nanocavities. *Nature* **2016**, *535*, 127–130.
- (34) Schnappinger, T.; Sidler, D.; Ruggenthaler, M.; Rubio, A.; Kowalewski, M. Cavity Born-Oppenheimer Hartree-Fock Ansatz: Light-Matter Properties of Strongly Coupled Molecular Ensembles. J. Phys. Chem. Lett. **2023**, 14, 8024–8033.
- (35) Vu, N.; McLeod, G. M.; Hanson, K.; De-Prince, A. E. Enhanced Diastereocontrol via Strong Light–Matter Interactions in an Optical Cavity. *J. Phys. Chem. A* **2022**, *126*, 9303–9312.
- (36) Yang, J.; Ou, Q.; Pei, Z.; Wang, H.; Weng, B.; Shuai, Z.; Mullen, K.; Shao, Y. Quantum-electrodynamical time-dependent density functional theory within Gaussian atomic basis. J. Chem. Phys. 2021, 155, 064107.
- (37) Yang, J.; Pei, Z.; Leon, E. C.; Wickizer, C.; Weng, B.; Mao, Y.; Ou, Q.; Shao, Y. Cavity quantum-electrodynamical time-dependent density functional theory within Gaussian atomic basis. II. Analytic energy gradient. The Journal of Chemical Physics 2022, 156, 124104.
- (38) McTague, J.; Foley, J. J. Non-Hermitian cavity quantum electrodynamics—configuration interaction singles approach for polaritonic structure with ab initio molecular Hamiltonians. J. Chem. Phys. 2022, 156, 154103.
- (39) Pavošević, F.; Flick, J. Polaritonic Unitary Coupled Cluster for Quantum Computations. J. Phys. Chem. Lett. **2021**, 12, 9100–9107.